

Kosterlitz-Thouless Crossover on a Two-Dimensional Lattice of Josephson-Coupled Bose-Einstein Condensates

V. Schweikhard, S. Tung, and E. A. Cornell[*]

*JILA, National Institute of Standards and Technology and University of Colorado,
and Department of Physics, University of Colorado, Boulder, Colorado 80309-0440*

(Dated: January 26, 2014)

We observe the Kosterlitz-Thouless crossover in a two-dimensional array of Josephson-coupled Bose-Einstein condensates. As long as the Josephson (tunneling) energy J exceeds the thermal energy T , i.e. $J/T \gtrsim 1$, the array is vortex-free. With decreasing J/T , vortices appear in the system, destroying long-range phase coherence. We confirm thermal activation as the vortex formation mechanism and obtain information on the size of bound vortex pairs as J/T is varied.

PACS numbers: 03.75.Lm, 03.75.Gg, 74.50.+r, 74.81.Fa, 67.90.+z

One of the defining characteristics of superfluids is long-range phase coherence [1]. Processes that destroy phase coherence are of both fundamental and technological interest and are particularly amenable to study in ultracold quantum gases. Fundamental underlying mechanisms may be quantum fluctuations, as in the Mott-insulator transition [2, 3], or thermal fluctuations, e.g. in one-dimensional Bose gases [4, 5] and in a double-well system [6]. In two dimensions (2D), Berezinskii [7], Kosterlitz and Thouless [8] (BKT) developed an elegant description of thermal phase fluctuations based on the unbinding of vortex-antivortex pairs, i.e. pairs of vortices of opposite circulation. The BKT picture applies to a wide variety of 2D systems, among them Josephson junction arrays (JJA), i.e. arrays of superfluids in which phase coherence is mediated via a tunnel coupling J between adjacent sites. Placing an isolated (*free*) vortex into a JJA is thermodynamically favored if its free energy $F = E - TS \leq 0$. In an array of period d the vortex energy diverges with array size R as $E \approx J \log(R/d)$ [9], but may be offset by an entropy gain $S \approx \log(R/d)$ due to the available $\approx R^2/d^2$ sites. This leads to a critical condition $(J/T)_{crit} \approx 1$ independent of system size, below which free vortices will proliferate and their large scale phase disturbances will destroy phase coherence. In contrast, *bound* vortex-antivortex pairs create localized phase disturbances and have little effect on phase coherence. Due to their small energy cost, such pairs show up even above $(J/T)_{crit}$, their density and size growing smoothly with decreasing J/T . Hence many, but not all, characteristics of the BKT transition vary rather smoothly with J/T .

Measurements of macroscopic response, both in continuous superfluids [10, 11] and superconducting JJA [12] have confirmed the predictions of BKT, without however directly observing its microscopic mechanism, vortex-antivortex unbinding. A recent study in a continuous 2D Bose gas showed the connection between vortex activation and phase fluctuations [13].

Here we report on the study of the BKT crossover in a 2D array of Josephson-coupled Bose-Einstein condensates (BEC). This system was studied theoretically in [14]. Our experiment starts with production of a partially Bose-condensed sample of ^{87}Rb atoms in a har-

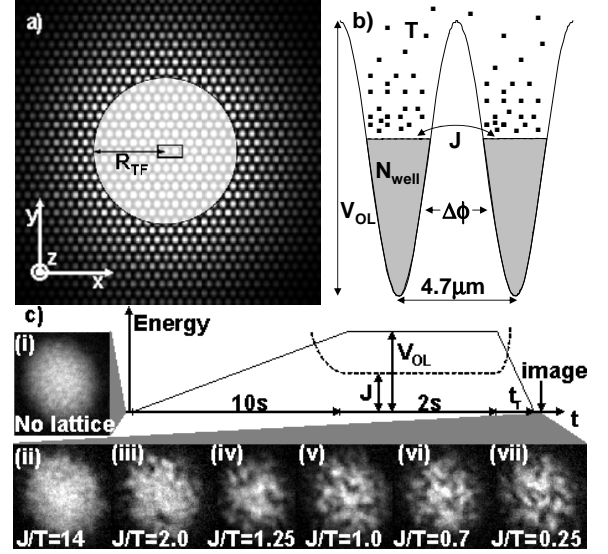


FIG. 1: Experimental system. (a) 2D optical lattice intensity profile. A lattice of Josephson-coupled BECs is created in the white-shaded area. The central box marks the basic building block of our system, the double-well potential shown in (b). The barrier height V_{OL} and the number of condensed atoms per well, N_{well} , control the Josephson coupling J , which acts to lock the relative phase $\Delta\phi$. A cloud of uncondensed atoms at temperature T induces thermal fluctuations and phase defects in the array when $J < T$. (c) Experimental sequence: A BEC (i) is loaded into the optical lattice over 10 s, suppressing J to values around T . We allow 2 s for thermalization. To probe the system, the lattice is ramped off on a fast timescale t_r [22] and images of the recombined condensate are taken. When J is reduced below T (ii)-(vii), vortices (dark spots) appear as remnants of the thermal fluctuations in the array.

monic, axially symmetric magnetic trap with oscillation frequencies $\{\omega_{x,y}, \omega_z\} = 2\pi\{6.95, 15.0\}$ Hz. The number of *condensed* atoms is kept fixed around 6×10^5 as the temperature is varied. We then transform this system into a Josephson junction array, as illustrated in Fig.1. In a 10 s linear ramp, we raise the intensity of a 2D hexagonal optical lattice [15] of period $d = 4.7\mu\text{m}$ in the x - y plane. The resulting potential barriers of height V_{OL} be-

tween adjacent sites [Fig.1(b)] rise above the condensate's chemical potential around $V_{OL} \approx 250 - 300 \text{ Hz}$, splitting it into an array of condensates which now communicate only through tunneling. This procedure is adiabatic even with respect to the longest-wavelength phonon modes of the array [17, 18] over the full range of V_{OL} in our experiments. Each of the ≈ 190 occupied sites (15 sites across the BEC diameter $2 \times R_{TF} \approx 68 \mu\text{m}$ [19]) now contains a macroscopic BEC, with $N_{well} \approx 7000$ condensed atoms in each of the central wells at a temperature T that can be adjusted between $30 - 70 \text{ nK}$. By varying V_{OL} in a range between 500 Hz and 2 kHz we tune J between $1.5 \mu\text{K}$ and 5 nK , whereas the “charging” energy E_c is on the order of a few $p\text{K}$, much smaller than both J and T . In this regime, thermal fluctuations of the relative phases $\Delta\phi_{Th} = \sqrt{T/J}$ are expected, while quantum fluctuations $\Delta\phi_Q = (E_c/4J)^{1/4}$ are negligible [1].

The suppression of the Josephson coupling greatly suppresses the energy cost of phase fluctuations in the x-y plane, *between* condensates, $J[1 - \cos(\Delta\phi)]$, compared to the cost of axial (z) phase fluctuations *inside* the condensates [20]. As a result, axial phase fluctuations remain relatively small, and each condensate can be approximated as a single-phase object [21].

After allowing 2 s for thermalization, we initiate our probe sequence. We first take a nondestructive thermometry image in the x-z plane, from which the temperature T of the sample and, from the axial condensate size R_z , the number of condensed particles per well, N_{well} , is obtained (see below). To observe the phase fluctuations we then turn down the optical lattice on a time-scale t_r [22], which is fast enough to trap phase winding defects, but slow enough to allow neighboring condensates to merge, provided their phase difference is small. Phase fluctuations are thus converted to vortices in the reconnected condensate, as has been observed in the experiments of Scherer *et al.* [23]. We then expand the condensate by a factor of 6 and take a destructive image in the x-y plane.

Figure 1(c) illustrates our observations: (ii)-(vii) is a sequence of images at successively smaller J/T (measured in the center of the array [24]). Vortices, visible as dark “spots” in (iii)-(vii), occur in the BEC center around $J/T = 1$. Vortices at the BEC edge appear earlier, as here the magnetic trap potential adds to the tunnel barrier, suppressing the *local* J/T below the quoted value. That the observed “spots” are indeed circulation-carrying vortices and antivortices can be inferred from their $\approx 100 \text{ ms}$ decay after the optical lattice ramp-down, presumably dominated by vortex-antivortex annihilation. A circulation-free hole would be filled within 3 ms by mean field dynamics, while vortices with identical circulation would decay by dissipative motion to the BEC edge, in our trap over $\gtrsim 10 \text{ s}$. Note the striking similarity of the images to recent numerical simulations of the BKT crossover in a continuous 2D Bose gas [25].

To investigate the thermal nature of phase fluctuations, in particular the scaling $J_{crit} \propto T$, we observe the crossover by varying J at different temperatures. For

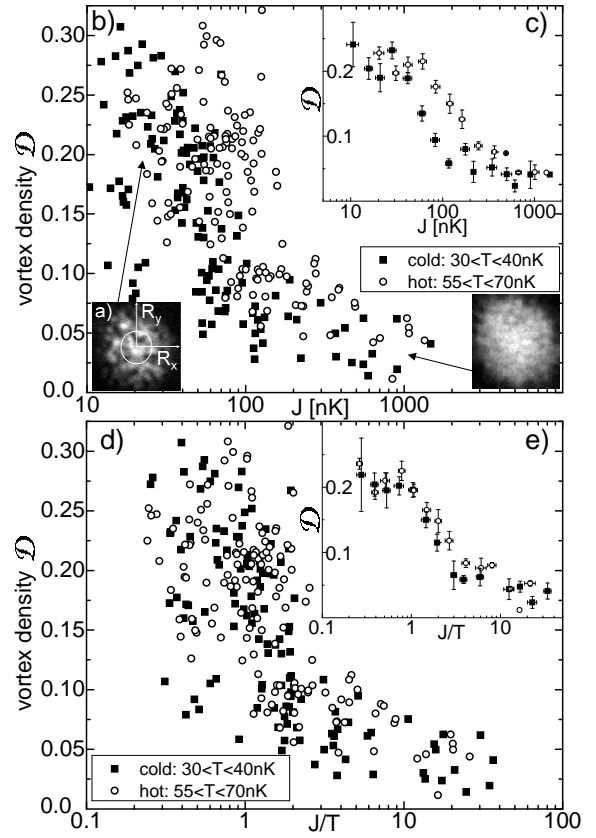


FIG. 2: Quantitative study of vortices. The areal density of vortices is quantified by the plotted \mathcal{D} defined in the text. \mathcal{D} is extracted only from the central 11% of the condensate region [circle in inset (a)] to minimize effects of spatial inhomogeneity. (b) \mathcal{D} vs J for two datasets with distinct “cold” and “hot” temperatures. Each point represents one experimental cycle. The increase in \mathcal{D} with decreasing $J \lesssim 100 \text{ nK}$ signals the appearance of vortices and the BKT crossover, while the “background” $\mathcal{D} \lesssim 0.1$ for $J \gtrsim 200 \text{ nK}$ is not associated with vortices. The crossover clearly occurs at larger J for the “hot” data, indicating thermal activation as the vortex formation mechanism. The large scatter in \mathcal{D} below the crossover is due to shot noise on the small average number of vortices in the central condensate region. (c) same data as in (b), but averaged within bins of size $\Delta[\log(J)] = 0.15$. Error bars of \mathcal{D} are standard errors. (d) same data as (b), but plotted vs J/T . The “cold” and “hot” datasets almost overlap, as confirmed by averaging [inset (e)], clearly identifying the competition of J and T as the cause of the crossover.

a quantitative study, accurate parameter estimates are required. The Josephson-coupling energy J is obtained from 3D numerical simulations of the Gross-Pitaevskii equation (GPE) for the central double-well system [6, 26] [Fig.1(b)], self-consistently including mean-field interactions of both condensed and uncondensed atoms [27]. A useful approximation for J in the crossover region is [24]: $J(V_{OL}, N_{well}, T) \approx N_{well} \times 0.315 \text{ nK} \exp[N_{well}/3950 - V_{OL}/244 \text{ Hz}](1 + 0.59 T/100 \text{ nK})$. The finite T correction to J arises from both the lifting-up of the BEC's chemical potential and the axial compression by the thermal

cloud's repulsive mean field, but does *not* take into account the effects of phase fluctuations on J (in condensed-matter language, we calculate the *bare* J). N_{well} is determined by comparison of the experimentally measured R_z , to $R_z(V_{OL}, N_{well}, T)$ obtained from GPE simulations. Both experimental and simulated R_z are obtained from a fit to the distribution of condensed and uncondensed atoms, to a Thomas-Fermi profile plus mean-field-modified Bose function [27]. In determination of all J values, there is an overall systematic multiplicative uncertainty $\Delta J/J = \approx 1.6$, dominated by uncertainties in the optical lattice modulation contrast, the absolute intensity calibration, and magnification in the image used to determine N_{well} . In comparing J for “hot” and “cold” clouds (see Fig. 2) there is a relative systematic error of 15% associated with image fitting and theory uncertainties in the thermal-cloud mean-field correction to J .

Figure 2 shows results of our quantitative study. The plotted quantity \mathcal{D} is a robust measure of the areal density of vortices. We define \mathcal{D} as the root-mean-square deviation per unit area of the measured column density from a fit to a Thomas-Fermi profile plus mean-field-modified Bose function, normalized by the fitted condensate peak column density. Several steps are taken to purify \mathcal{D} from undesired effects: Images are binned such that one pixel corresponds to 40% of the full width at half maximum of a centered isolated vortex with good contrast. To limit inhomogeneous broadening of the crossover, caused by spatially inhomogeneous condensate density and optical lattice intensity, to less than 10%, \mathcal{D} is extracted only from the central 11% of the condensate area, see Fig. 2(a). Finally, an offset $\mathcal{D}_0 = 0.067$ (measured for BECs with no optical lattice applied) is subtracted in quadrature from \mathcal{D} to approximately remove contributions from fit imperfections and image noise.

In Fig. 2(b), we plot \mathcal{D} vs J for two datasets with distinct temperatures. At large $J \gtrsim 200 nK$ a background $\mathcal{D} \lesssim 0.1$ is observed, that is not associated with vortices, but due to residual density ripples remaining after the optical lattice ramp-down. The BKT crossover, signaled by a rise of \mathcal{D} above ≈ 0.1 , occurs around $J \approx 100 nK$ for “hot” BECs and at a distinctly lower $J \approx 50 nK$ for “cold” BECs [confirmed by the averaged data shown in Fig. 2(c)], indicating thermal activation as the vortex formation mechanism. The large fluctuations in \mathcal{D} at small J are due to shot noise on the small average number of vortices in the central 11% of the condensate area (well below the crossover, a vortex-counting routine finds, on average, 3.5 vortices). Comparison with vortex-counting results shows that \mathcal{D} is approximately linearly related to the number of vortices in the central condensate region, with a sensitivity of ≈ 0.04 per vortex and an offset of ≈ 0.06 not associated with vortices. Plotting the same data vs J/T in Fig. 2(d) shows collapse onto a universal curve, providing strong evidence for thermal activation. A slight residual difference becomes visible in the averaged “cold” vs “hot” data [Fig. 2(e)], perhaps because of systematic differences in our determination of

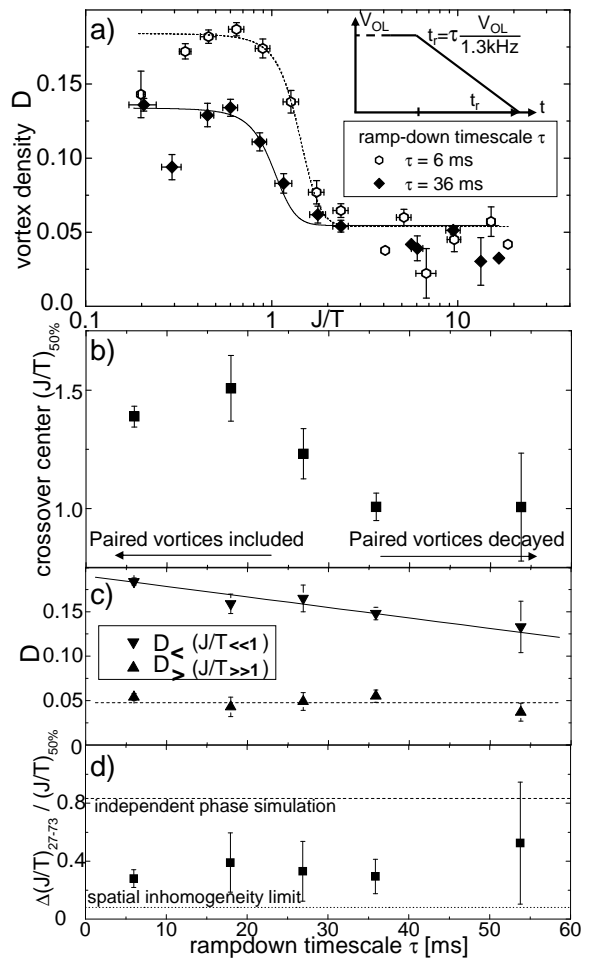


FIG. 3: (a) Vortex density \mathcal{D} probed at different optical lattice ramp-down timescales τ . A slow ramp provides time for tightly bound vortex pairs to annihilate, allowing selective counting of loosely bound or free vortices only, whereas a fast ramp probes both free and tightly bound vortices. A fit to a smooth functional form determines the midpoint of the crossover $(J/T)_{50\%}$, its 27% – 73% width $\Delta(J/T)_{27-73}$, and the limiting values $\mathcal{D}_<$ ($\mathcal{D}_>$) well below (above) $(J/T)_{50\%}$. (b) A downshift in $(J/T)_{50\%}$ is seen for slow ramps, consistent with the occurrence of loosely bound or free vortices at lower J/T only. The limiting $(J/T)_{50\%} \approx 1$ for slow ramps possibly reveals the true BKT vortex unbinding. (c) $\mathcal{D}_>$ (\blacktriangle) and $\mathcal{D}_<$ (\blacktriangledown) as a function of ramp time τ . (d) Relative crossover width $\Delta(J/T)_{27-73} / (J/T)_{50\%}$ compared to simulation results for an array of phases independently fluctuating as $\Delta\phi_{RMS} = \sqrt{T/J}$, and the limit set by spatial inhomogeneity.

J at different temperatures.

The flexibility of optical potentials allows us to probe the microscopic BKT picture in more detail, distinguishing free vortices from tightly bound pairs. A “slow” optical lattice ramp-down allows time for tightly bound vortex pairs to annihilate before they can be imaged. By slowing down the ramp duration τ [inset of Fig. 3 (a)], we therefore selectively probe vortices at increasing spatial scales and most importantly approach the “true” BKT

vortex-unbinding crossover in the limit of slow ramps.

Figure 3(a) shows the crossover, probed at two different ramp times. Two points are worth noticing: First, a slow ramp compared to a fast one shows a reduction of the vortex density in arrays with fully randomized phases at low J/T . The difference directly shows the fraction of tightly bound pairs that annihilate on the long ramp. Second, a slower ramp exhibits the crossover at lower $(J/T)_{50\%}$, confirming that free or very loosely bound vortices occur only at higher T (lower J). Specifically, the data clearly show a range around $J/T \approx 1.4$ where only tightly bound pairs exist. Figure 3(b) quantitatively shows the shift of $(J/T)_{50\%}$ from 1.5 to 1 with slower ramp time. We can make a crude mapping of the experimental ramp-down time-scale to theoretically more accessible length-scales as follows: From Fig. 3(c), we see that the saturated (low- J/T) vortex density ($\mathcal{D}_< - \mathcal{D}_>$) for $\tau = 60\text{ ms}$ ramps decreases to 1/2 of its value for fast ramps, i.e. the most tightly bound 50% of vortices annihilate. Simulations [28] show that in a fully randomized hexagonal array, after excluding pairs so tightly bound that they presumably annihilate even during the fastest ramps, about 50% of vortices are within $1.3 \times d$ of a vortex with opposite circulation. Thus we infer that ramps of $\tau = 60\text{ ms}$ or longer allow time for bound pairs of spacing less than $1.3 \times d$ to decay before we observe them. The downward shift of $(J/T)_{50\%}$ in Fig. 3(b) thus tells us that vortex pairs bound more tightly than $1.3 \times d$ appear in large number for $J/T \leq 1.5$, whereas more loosely bound

pairs, or indeed free vortices, do not appear in quantity until $J/T \leq 1$; thus $(J/T)_{50\%} = 1.0 \times 1.6$ appears to be close to the “true” BKT crossover, inviting a theoretical investigation including finite-size and array geometry effects.

A further interesting observation concerns the width of the crossover. Figure 3(d) shows the relative width of the crossover, $\Delta(J/T)_{27-73}/(J/T)_{50\%} \approx 0.3$, which is independent of ramp-down duration. This width is neither as broad as in a double-well system [6, 29], where the coherence factor rises over a range $\Delta(J/T)_{27-73}/(J/T)_{50\%} \approx 1.4$, nor as broad as expected from simulations [28] of an array of independently fluctuating phases $\Delta\phi_{RMS} = \sqrt{T/J}$, where $\Delta(J/T)_{27-73}/(J/T)_{50\%} \approx 0.85$. Presumably collective effects in the highly multiply connected lattice narrow the transition. On the other hand, the width is 3 – 4 times larger than the limit due to spatial inhomogeneity in J , suggesting contributions to the width due to finite-size effects or perhaps arising from the use of vortex density as the signature of the crossover.

In conclusion, we have probed the BKT crossover in a 2D lattice of Josephson-coupled BECs by studying thermally driven vortex formation. Allowing variable time for vortex-antivortex pair annihilation before probing the system provides a time-to-length mapping, which reveals information on the size of pairs with varying J/T . We acknowledge illuminating conversations with Leo Radzihovsky and Victor Gurarie. This work was funded by NSF and NIST.

-
- [*] Quantum Physics Division, National Institute of Standards and Technology.
- [1] A. Leggett, *Rev. Mod. Phys.* **73**, 307 (2001).
- [2] M. Greiner *et al.*, *Nature* **415**, 39 (2002).
- [3] D. Jaksch *et al.*, *Phys. Rev. Lett.* **81**, 003108 (1998).
- [4] S. Richard *et al.*, *Phys. Rev. Lett.* **91**, 010405 (2003);
- [5] D. Hellweg *et al.*, *Phys. Rev. Lett.* **91**, 010406 (2003).
- [6] R. Gati *et al.*, *Phys. Rev. Lett.* **96**, 130404 (2006).
- [7] V. Berezinskii, *Sov. Phys.-JETP* **32**, 493 (1971); **34**, 610 (1972).
- [8] J. Kosterlitz, D. Thouless, *J. Phys. C* **6**, 1181 (1973).
- [9] M. Tinkham, *Introduction to Superconductivity*, McGraw-Hill, Inc., New York (1996).
- [10] G. Agnolet *et al.*, *Phys. Rev. B* **39**, 8934 (1989).
- [11] A. Safonov *et al.*, *Phys. Rev. Lett.* **81**, 4545 (1998).
- [12] D. Resnick *et al.*, *Phys. Rev. Lett.* **47**, 1542 (1981).
- [13] Z. Hadzibabic *et al.*, *Nature* **441**, 1118 (2006).
- [14] A. Trombettoni *et al.*, *New J. Phys.* **7**, 57 (2005).
- [15] Three circularly polarized laser beams ($\lambda = 810\text{ nm}$) intersect in a tripodlike configuration, with $\theta = 6.6^\circ$ angles to the z -axis. Calculation of the optical dipole potential [16] includes counterrotating terms and interaction with both the D1 and D2 lines, as well as the ‘fictitious magnetic field’ due to the circular polarization. The tilted bias field of the TOP trap makes $\mathcal{P} \approx 0.5$ [16].
- [16] R. Grimm *et al.*, *Adv. At. Mol. Opt. Phys.* **42**, 95 (2000).
- [17] J. Javanainen, *Phys. Rev. A* **60**, 4902 (1999).
- [18] K. Burnett *et al.*, *J. Phys. B* **35**, 1671 (2002).
- [19] To avoid radial flows during V_{OL} ramp-up, R_{TF} is kept constant by balancing the lattice-enhanced mean field pressure with radial confinement due to the optical lattice envelope, by the choice of a $67\mu\text{m}$ $1/e^2$ intensity waist. Axial (z) confinement is due to the magnetic trap alone.
- [20] D. Petrov *et al.*, *Phys. Rev. Lett.* **87**, 050404 (2001).
- [21] In the axial condensate region between $z = -R_z/3, +R_z/3$, where according to our 3D GPE simulations 85% of the tunnel current is localized and hence the relative phase is measured, axial phase fluctuations [20] vary between $\approx 600\text{ mrad}$ (“cold” data in Fig. 1) and 800 mrad (“hot”) in the crossover regime $J/T \approx 1$.
- [22] Within a dataset, the ramp-down rate is kept fixed, $t_r = \tau \times V_{OL}/1.3\text{ kHz}$, $\tau = 18\text{ ms}$ if not otherwise indicated.
- [23] D. Scherer *et al.*, *Phys. Rev. Lett.* **98**, 110402 (2007).
- [24] J is averaged over junctions within the central 11% of the array area, from which all quantitative experimental results are extracted.
- [25] T. Simula and P. Blakie, *Phys. Rev. Lett.* **96**, 020404 (2006).
- [26] D. Ananikian and T. Bergeman, *Phys. Rev. A* **73**, 013604 (2006).
- [27] M. Naraschewski and D. Stamper-Kurn, *Phys. Rev. A* **58**, 2423 (1998).
- [28] Following [23], in simulations we count a vortex if all three phase differences in an elemental triangle of junctions are between 0 and π , or if all are between 0 and $-\pi$.

We discard vortex-antivortex pairs in adjacent triangles (spaced by $\approx 0.6 \times d$), which presumably annihilate before we can image them even for fast ramps. Including these pairs would produce more than $2\times$ disagreement

with experimental vortex counts for $J/T \ll 1$.
 [29] L. Pitaevskii and S. Stringari, Phys. Rev. Lett. **87**, 180402 (2001).